THE JOURNAL OF BIOLOGICAL CHEMISTRY VOL. 289, NO. 33, pp. 22850–22864, August 15, 2014

5′-AMP-activated Protein Kinase (AMPK) Supports the Growth of Aggressive Experimental Human Breast Cancer Tumors*

Received for publication, May 5, 2014, and in revised form, June 20, 2014 Published, JBC Papers in Press, July 3, 2014, DOI 10.1074/jbc.M114.576371

Keith R. Laderoute[‡1], Joy M. Calaoagan[‡2], Wan-ru Chao[‡], Dominc Dinh[‡], Nicholas Denko[§], Sarah Duellman[‡3], Jessica Kalra[¶], Xiaohe Liu[‡], Ioanna Papandreou[§], Lidia Sambucetti[‡], and Laszlo G. Boros[‖‡‡]**

*From the [‡]Biosciences Division, SRI International, Menlo Park, California 94025, the [§]Department of Radiation Oncology, The James Comprehensive Cancer Center, Ohio State University, Columbus, Ohio 43210, the [¶]Department of Biology, Langara College, Vancouver, British Columbia V5W 2Z6, Canada, the [‖]Department of Pediatrics, UCLA School of Medicine, Los Angeles, California 90509, the **Los Angeles Biomedical Research Institute at the Harbor-UCLA Medical Center, Torrance, California 90502, and [‡‡]SIDMAP, LLC, Los Angeles, California 90064*

Background: 5′-AMP-activated protein kinase (AMPK) is a ubiquitous regulator of cellular energy homeostasis.
Results: AMPK contributes to the growth and core glucose metabolism of aggressive (rapidly growing) experimental human tumors.
Conclusion: AMPK can be activated by metabolic stress to support the growth of aggressive tumors.
Significance: AMPK's role in tumor biology could be strongly influenced by microenvironmental stress.

Rapid tumor growth can establish metabolically stressed microenvironments that activate 5′-AMP-activated protein kinase (AMPK), a ubiquitous regulator of ATP homeostasis. Previously, we investigated the importance of AMPK for the growth of experimental tumors prepared from *HRAS*-transformed mouse embryo fibroblasts and for primary brain tumor development in a rat model of neurocarcinogenesis. Here, we used triple-negative human breast cancer cells in which AMPK activity had been knocked down to investigate the contribution of AMPK to experimental tumor growth and core glucose metabolism. We found that AMPK supports the growth of fast-growing orthotopic tumors prepared from MDA-MB-231 and DU4475 breast cancer cells but had no effect on the proliferation or survival of these cells in culture. We used *in vitro* and *in vivo* metabolic profiling with [^{13}C]glucose tracers to investigate the contribution of AMPK to core glucose metabolism in MDA-MB-231 cells, which have a Warburg metabolic phenotype; these experiments indicated that AMPK supports tumor glucose metabolism in part through positive regulation of glycolysis and the nonoxidative pentose phosphate cycle. We also found that AMPK activity in the MDA-MB-231 tumors could systemically perturb glucose homeostasis in sensitive normal tissues (liver and pancreas). Overall, our findings suggest that the contribution of AMPK to the growth of aggressive experimental tumors has a critical microenvironmental component that involves specific regulation of core glucose metabolism.

Both inherent (cell autonomous) and microenvironmental influences favor the emergence of metabolism in tumor cells that is fundamentally different from that in most normal cells (1–3). Indeed, the unique energy metabolism associated with transformation is considered a hallmark of human cancer (4). Perhaps the most commonly observed inherent metabolic phenotype of tumor cells is the Warburg effect, in which glucose is consumed by glycolysis with substantial lactate production even in the presence of abundant oxygen (aerobic glycolysis) (1, 3). The Warburg effect is considered an important mechanism by which tumor cells divert glucose flux from catabolism by oxidative phosphorylation to anabolism (biomass production), thus supporting cellular growth and proliferation at the cost of efficient ATP production. At the tissue level, the growth of solid tumors commonly generates regions of nutrient or metabolic stress (*e.g.* hypoxia, glucose deprivation, and acidification); tumor cells in these regions may exhibit a microenvironmental Warburg-like effect (2, 5). Research to understand the molecular basis of such phenotypes has revealed that key metabolic regulators are important contributors to tumor cell metabolism (1, 2). We have been interested in understanding the role of 5′-AMP-activated protein kinase (AMPK),[4] a master regulator of cellular energy metabolism (6, 7), in the development of tumors that contain metabolically stressed microenvironments. In previous research, we found that AMPK is activated by tumor-like hypoxia and glucose stress in cultures of transformed cells and that AMPK activity is abundant in experimental rodent tumors such as mouse fibrosarcoma xenografts and rat primary brain tumors (8, 9). The mouse fibrosarcomas were prepared from *HRAS* G12V-transformed mouse embryo fibroblasts in which AMPK activity was intact (control) or eliminated by disruption (knock-out/KO) of the two genes for the

* This work was supported, in whole or in part, by National Institutes of Health Grants HHSN261200800001E and CA73807 from NCI.
[1] To whom correspondence should be addressed. E-mail: keith.laderoute@sri.com.
[2] Present address: Imago BioSciences, San Carlos, CA 94070.
[3] Present address: Promega Corp., Madison, WI 53711.

[4] The abbreviations used are: AMPK, 5′-AMP-activated protein kinase; BisTris, 2-[bis(2-hydroxyethyl)amino]-2-(hydroxymethyl)propane-1,3-diol; CB, cytochalasin B; PPC, pentose phosphate cycle; qPCR, quantitative RT-PCR; KD, knockdown; TCA, tricarboxylic acid; TK, transketolase; KD, knockdown; TN, triple-negative; EI, electron impact ionization.

AMPKα catalytic subunits (*Prkaa1*, *Prkaa2*; AMPKα1/2 KO cells); we found that growth of the KO tumors was almost suppressed compared with growth of the control tumors. In contrast, we found that AMPK activity was dispensable for the proliferation or survival of the same cell lines in nutrient-rich (normal) culture medium (8).

Here, we describe studies to investigate the importance of AMPK for both the growth and core glucose metabolism of aggressive (rapidly growing) experimental human breast cancer tumors. In particular, we used knockdown (KD) technology to inhibit expression of both the *PRKAA1* and *PRKAA2* genes in the MDA-MB-231 cell line, which is a commonly used model of triple-negative (TN) or advanced breast cancer (10, 11), and prepared orthotopic tumor xenografts in nude mice from the control and AMPKα1/2 KD cell lines. We found that KD of AMPK activity in these cells generated the same *in vivo* and *in vitro* phenotypes as KO of AMPK activity in *HRAS* G12V-transformed mouse embryo fibroblasts, *i.e.* poor growth as tumors in nude mice, but no significant effect on the proliferation or survival of the same cells under nutrient-rich culture conditions. We confirmed these two AMPKα1/2 KD phenotypes by using a different TN human breast cancer cell line (DU4475 cells). Because MDA-MB-231 cells have a documented Warburg effect (12), we used these cells for metabolic profiling with ^{13}C-labeled D-glucose (glucose) to investigate the contribution of AMPK to core glucose metabolism both *in vitro* (cell culture) and *in vivo* (orthotopic tumors). We found that glucose utilization in AMPKα1/2 KD compared with control MDA-MB-231 tumors resembled a non-Warburg metabolic phenotype; importantly, this *in vivo* phenotype retained specific AMPK-dependent effects on core glucose metabolism detected by *in vitro* metabolic profiling of the same cells. Finally, we observed AMPK-dependent effects of MDA-MB-231 tumor burden on glucose metabolism in normal liver and pancreas, which indicated a systemic interaction between tumor- and glucose-responsive normal tissues. Overall, our findings suggest the general hypothesis that AMPK could support the growth and core glucose metabolism of aggressive human tumors containing metabolically stressed microenvironments.

EXPERIMENTAL PROCEDURES

Materials—Goat polyclonal anti-AMPKα1 and -α2 antibodies were obtained from Santa Cruz Biotechnology (Santa Cruz, CA; catalog nos. sc-19128 and sc-19131, respectively). The following rabbit polyclonal antibodies were obtained from Cell Signaling Technology: an AMPKα1/2 (AMPKα) antibody (catalog no. 2532S); an acetyl-CoA carboxylase antibody (catalog no. 3662S); and a phospho-Ser-79 acetyl-CoA carboxylase 1 antibody (3661L). A lentivirus preparation containing shRNAs for targeting human AMPKα1/2 expression was obtained from Santa Cruz Biotechnology (AMPKα1/2 shRNA (h) Lentiviral Particles; catalog no. sc-45312-V). The lentivirus preparation consists of pools of three target-specific constructs that encode 28 nucleotide (plus hairpin) shRNAs for each of the AMPKα1 and -α2 mRNAs (*PRKAA1/2* mRNAs). A lentivirus preparation containing a nonsense/scrambled shRNA was used as a negative control for these studies (control shRNA lentiviral particles, Santa Cruz Biotechnology, catalog no. sc-108080).

Cell Culture—MDA-MB-231-lucD3H2LN human breast cancer cells (called MDA-MB-231 cells below) were obtained from PerkinElmer Life Sciences/Caliper (Hopkinton, MA; MDA-MB-231-luc-D3H2LN Bioware Cell Line) (13). DU4475 human breast cancer cells were obtained from the American Type Culture Collection (ATCC) (HTB-123). These two breast cancer cell lines are classified as TN (10, 14). Cells were cultured in Dulbecco's modified Eagle's medium (DMEM) supplemented with 10% FBS and 25 mM HEPES (Invitrogen) at 37 °C in a humidified 5% CO_2/air atmosphere. Proliferation/viability of cell cultures was measured with an AlamarBlue assay (Invitrogen) (15) or by cell counting using a NucleoCounter device (ChemoMetec, Allerød, Denmark).

Generation of AMPKα1/2 KD Cell Lines—Cells were infected with the lentivirus preparation described above to generate shRNA control and AMPKα1/2 KD cell lines. Cells at ~50% confluency in a 24-well culture plate were exposed to lentivirus particles in complete medium containing Polybrene (5 μg/ml; Santa Cruz Biotechnology, catalog no. sc-134220); cells were typically infected at multiplicity of infection values of 10 or 40. Infected cells were incubated at 37 °C in 5% CO_2/air overnight, and the medium was replaced with complete medium for another overnight incubation. The medium was replaced with selection medium (containing 2 μg/ml puromycin; Invitrogen), and the selection medium was replaced every 3–4 days until resistant colonies appeared. Pooled colonies were expanded, and cells were cryopreserved or used immediately for experiments (culture medium was supplemented with 2 μg/ml puromycin). The extent of AMPKα1/2 KD in each cell line was monitored by immunoblotting and quantitative RT-PCR analyses; if changes in the extent of KD were detected with time in culture (passaging), early passage cells were obtained from frozen stocks for subsequent experiments.

Immunoblotting Analysis—Culture dishes or plates were placed on ice or on cold packs, and the medium was removed. Cells were lysed by adding ≤200 μl of lysis buffer (50 mM Tris-HCl, pH 7.4, 0.5% Nonidet P-40, 250 mM NaCl, 1 mM DTT, 50 mM NaF, 15 mM $Na_4P_2O_7$, 25 mM β-glycerophosphate, 1 mM Na_3VO_4, 100 nM okadaic acid (EMD/Millipore Chemicals, Darmstadt, Germany), 50 units benzonase nuclease (EMD/Millipore), 1× Protease Inhibitor Mixture III, PIC III (EMD/Millipore)). After spinning at 9,000 × *g* for 10 min at 4 °C, the protein concentrations of the supernatants were determined by using a bicinchoninic acid assay (Thermo Scientific, Rockford, IL). Equal protein samples (typically 10–15 μg) were resolved in 4–12% SDS-polyacrylamide gels (NuPAGE BisTris Gels, Invitrogen) and electroblotted onto Immobilon-FL membranes (EMD/Millipore). Blots were blocked in a 1:1 mixture of Odyssey Blocking Buffer (LI-COR Biosciences, Lincoln, NB) and PBS, pH 7.4, at 4 °C. For protein detection, blots were incubated overnight at 4 °C with a primary antibody typically diluted 1:1,000 in Odyssey Blocking Buffer containing 0.1% Tween 20. After washing with PBS containing 0.1% Tween 20, blots were incubated for 1 h at room temperature containing a species-specific IRDye 800-conjugated IgG antibody (LI-COR Biosciences) diluted (*e.g.* 1:10,000) in Odyssey Blocking Buffer containing 0.1% Tween 20 and 0.01% SDS. Primary antibody binding was detected and visualized by using an Odyssey Infra-

red Imaging System (LI-COR Biosciences). SeeBlue Plus 2 prestained standards (Invitrogen) were used to calibrate the immunoblots.

Quantitative RT-PCR (qPCR) Analysis—Total RNA was collected and purified by using an RNeasy mini kit (Qiagen, Valencia, CA) according to the supplier's instructions. First strand (cDNA) synthesis and qPCR were performed by using an RT^2 first strand kit and an RT^2 SYBER Green qPCR master mix kit from SABiosciences/Qiagen. Amplicons from the human AMPKα1/2 subunit gene mRNAs (*PRKAA1* and *PRKAA2*) were generated with the following primer sets (RT^2 qPCR primer assays, SABiosciences/Qiagen): *PRKAA1*, catalog no. PPH00043B (110-bp amplicon; located at position 1,537 in RefSeq sequence NM_006251) and *PRKAA2*, catalog no. PPH15207A (141-bp amplicon; located at position 1,530 in RefSeq sequence NM_006252). The amplicons were generated by using a LightCycler (Roche Applied Science) with the following thermocycling program: denaturation, 95 °C, 10 min; amplification, 95 °C, 15 s; annealing, 60 °C, 1 min; 45 cycles.

Tumor Xenografts—*In vivo* procedures were approved by the SRI Institutional Animal Care and Use Committee (IACUC). To investigate tumor growth, orthotopic tumors were initiated by injecting shRNA control or AMPKα1/2 KD cells (3×10^6 cells/cell line) in 100 μl of serum-free medium containing 50% Matrigel (BD Biosciences) into the right mammary fat pad (lower mammary papilla) of female nude mice (Harlan Laboratories, Livermore, CA). When the tumors reached a uniform mean volume (~100 mm^3), mice were separated into shRNA control and AMPKα1/2 KD groups (10–15 mice/group). Tumor growth was monitored daily, and tumor volumes were measured twice weekly (tumor volumes were calculated using the formula $V = L \times W \times H \times \pi/6$, where L and W represent the longer and shorter diameters of the tumor, and H represents the height of the tumor (16)). Analysis of tumor growth, including statistical comparisons between groups of mice, was performed using the Study Director package (Studylog Systems, Inc., South San Francisco) and GraphPad Prism/InStat (GraphPad Software, La Jolla, CA). One-way analysis of variance with a Tukey-Cramer post hoc test was used to determine the statistical significance of differences between the mean volumes of corresponding shRNA and AMPKα1/2 KD tumors; $p < 0.05$ was considered to indicate a significant difference between the mean tumor volumes of two groups. To investigate tumor metabolism, orthotopic tumors were prepared by injecting two groups of 30 mice each with shRNA control or AMPKα1/2 KD MDA-MB-231 cells. When the faster growing shRNA control tumors reached a mean volume of ~400 mm^3, metabolic profiling was performed using ^{13}C-labeled glucose, as described below.

A tumor cell colonization assay (also called an experimental metastasis assay) (17) was performed by injecting shRNA control or AMPKα1/2 KD MDA-MB-231 cells (2×10^6 cells/tail vein injection, suspended in serum-free medium; day 0) into groups of beige nude mice (Harlan Laboratories; 15 mice/group). The statistical significance of the survival data were evaluated by using the log-rank test. The distribution of the injected cells and the occurrence of tumors were monitored on day 0 and day 1, and then weekly for 10 weeks by bioluminescence imaging using an IVIS Lumina XR System (PerkinElmer Life Sciences/Caliper), according to the vendor's instructions. As mentioned above, the MDA-MB-231 cells constitutively express a luciferase reporter. Briefly, no later than 15 min before imaging, mice were injected i.p. with D-luciferin (PerkinElmer Life Sciences/Caliper) in Dulbecco's phosphate-buffered saline (D-PBS; without calcium and magnesium; Invitrogen) at 150 mg/kg/ml. Mice were anesthetized with sodium pentobarbital (60 mg/kg) during imaging. Image analysis was performed with Living Image software (PerkinElmer Life Sciences/Caliper), and bioluminescent signals were quantified as average signals (photon counts/s/cm^2) for comparisons between individual mice.

Steady-state Glucose and Glutamine Uptake Assays—Steady-state glucose uptake by cultured cells was measured essentially as described previously (18, 19). Cells were plated in 2 ml of medium in the wells of 6-well cell culture plates (1.5×10^5 cells/well) and incubated at 37 °C until they were ≤90% confluent. The cells were washed at least three times with D-PBS containing calcium and magnesium, and then 1 ml/well of D-PBS labeling solution was added (2 μCi/ml 2-deoxy-D-[1,2-^{3}H]glucose (PerkinElmer Life Sciences catalog no. NET549A250UC; 25–50 Ci/mmol; 1 mCi/ml), 0.1 mM 2-deoxy-D-glucose (Sigma, catalog no. D3179), 1% BSA; ±20 μM cytochalasin B (CB; Sigma, catalog no. C6762). The active glucose uptake inhibitor CB was used to control for passive diffusion of glucose into cells. Cells were incubated in the labeling solution at 37 °C for 10 min, and then they were placed on ice, and 1 ml/well of ice-cold D-PBS containing 110 μg/ml phloretin was added to stop active glucose uptake. Cells were washed three times with D-PBS containing 55 μg/ml phloretin and lysed by scraping in 0.3 ml/well of RIPA buffer (50 mM Tris buffer, pH 7.5, 150 mM NaCl, 0.1% SDS, 0.5% sodium deoxycholate, 1% Nonidet P-40 or Triton X-100, 1× protease inhibitor mixture (Roche Applied Science)). The lysates were spun at 12,000 rpm for 5 min, and protein concentrations were measured using a bicinchoninic acid (BCA) assay (Thermo Scientific). The radioactivities of the lysates were determined by counting 200 μl of each lysate in 4.5 ml of scintillation fluid, and the counts for lysates from CB-treated cells were subtracted from the counts for lysates from cells not treated with CB. Glucose uptake data were expressed as picomoles/mg of protein/5 min.

Steady-state L-glutamine (glutamine) uptake by cultured cells was measured by using L-[3,4-^{3}H]Glutamine ([^{3}H]glutamine; PerkinElmer Life Sciences; catalog no. NET551001MC; 30–60 Ci/mmol, 1 mCi/ml) as a tracer, essentially as described in Ref. 20. Cells were plated in 1 ml of medium in the wells of a 24-well cell culture plate (1.0×10^5 cells/well) and incubated at 37 °C until they were ≤90% confluent. The medium was replaced with medium containing 2 mM normal glutamine and 5 μCi of [^{3}H]glutamine, and the cells were incubated at 37 °C for 5 min. The plate was placed on ice, and the wells were washed five times with ice-cold PBS and air-dried for 20 min at room temperature. Cells were lysed by adding 210 μl/well of a solution of 0.2 N NaOH and 0.2% SDS, followed by the addition of 10 μl/well of 2 N HCl. The protein concentrations of the lysates were measured using a BCA assay, and radioactivity

measurements were made by counting 150 μl of each lysate in 4.5 ml of scintillation fluid. Glutamine uptake data were expressed as counts/min/mg total protein.

Measurement of Oxygen Consumption and Extracellular Acidification in Cell Cultures—Cells were plated in the wells of 96-well plates (1.5×10^5 cells/well; XF96 plates, Seahorse Bioscience, North Billerica, MA) and incubated at 37 °C overnight. The next day, the medium was changed to XF Assay Medium (Seahorse Bioscience) containing 25 mM glucose, 1 mM pyruvate, and 2 mM glutamine or containing 1 mM glucose, 0.05 mM pyruvate, and 2 mM glutamine, and the cells were incubated at 37 °C for 2 h. Steady-state (baseline) oxygen consumption rates and extracellular acidification rates were measured with an XF24 extracellular flux analyzer (Seahorse Bioscience). Addition of 2.5 μM oligomycin was used to evaluate the glycolytic response of the cells by inhibiting oxidative phosphorylation; addition of 5 μM carbonyl cyanide *m*-chlorophenyl hydrazone was used to evaluate the maximal respiratory response of the cells (21, 22).

Metabolic Profiling of ^{13}C-Labeled Glucose Metabolites—To investigate glucose metabolism in shRNA control and AMPKα1/2 KD MDA-MB-231 cells *in vitro*, subconfluent cultures of both genotypes (100-mm diameter culture plates; three replicates/cell line) were incubated with D-[1,2-$^{13}C_2$]glucose (called [$^{13}C_2$]glucose below; Sigma, catalog no. 661422-1G; 99 atom % ^{13}C) in glucose- and pyruvate-free DMEM (Sigma, catalog no. D5030). Cells were incubated in either high glucose medium (DMEM + 10% FBS; 25 mM glucose composed of 50% normal glucose and 50% [$^{13}C_2$]glucose) or low glucose medium (DMEM + 10% FBS; 1 mM glucose composed of 50% normal glucose and 50% [$^{13}C_2$]glucose) for 48 h, with one change of medium at 24 h. Cells were placed on ice; the medium was removed and frozen at −80 °C; cells were washed twice with ice-cold PBS; and cell pellets were prepared by trypsinization (pellets were stored at −80 °C).

To investigate glucose metabolism in orthotopic tumors prepared from shRNA control and AMPKα1/2 KD MDA-MB-231 cells, mice were injected i.p. (1 g/kg) with [$^{13}C_6$]glucose (D-[$^{13}C_6$]glucose, Sigma, catalog no. 389374-2G; 99 atom % ^{13}C) dissolved in sterile PBS (0.25 g/ml glucose; 50% [$^{13}C_6$]glucose/normal glucose). Blood samples were collected at 30, 60, and 90 min after completion of the glucose injections (blood was collected in EDTA-treated tubes and centrifuged at 5,000 rpm for 5 min; the plasma was stored at −80 °C). Mice used to collect blood at each time point were euthanized with sodium pentobarbital (60–80 mg/kg). Tumor, pancreas, and liver were immediately removed from each mouse; flash-frozen in liquid nitrogen; and stored at −80 °C.

CO_2 was obtained from culture medium (100 μl) or tissue (≤100 mg) by adding an equal volume of 0.1 M $NaHCO_3$ and 1 N HCl to a sample in a gas chromatography (GC) vial, followed immediately by analysis of the head space gas by mass spectrometry (GC-MS; see below for details). $^{12/13}CO_2$ isotopomers were monitored at *m/z* 44 and 45 in the electron impact ionization (EI) spectrum to determine the fraction of [$^{12/13}$C]glucose ([$^{13}C_2$]glucose or [$^{13}C_6$]glucose) that was completely oxidized by the pentose phosphate cycle (PPC) and the tricarboxylic acid (TCA) cycle, relative to $^{12}CO_2$ from the β-oxidation of (unlabeled) fatty acids (23–25). L-Lactate (lactate) was obtained from culture medium (2 ml) by acidification with 2 N HCl, extraction with ethylene chloride, and derivatization to the *n*-propylamide-heptafluorobutyric ester (24, 25). Lactate was obtained from tissue fragments (≤100 mg) by homogenization in 1 ml of TRIzol reagent (Invitrogen) according to the supplier's instructions; the aqueous phase of the homogenate was acidified with 2 N HCl (*e.g.* for 2 h), neutralized, and extracted with ethyl acetate; and the extracted lactate was derivatized to the *n*-propylamide-heptafluorobutyric ester. [$^{12/13}$C]Lactate isotopomers were monitored by GC-MS at the ion cluster at *m/z* 328 in the chemical ionization spectrum (carbons 1–3 of derivatized lactate) to detect metabolites with 1, 2, or 3 ^{13}C atoms from a [^{13}C]glucose tracer (M_1, M_2, and M_3 isotopomers, respectively, depending on the tracer). Together, these data were used to determine the relative contributions of the PPC and glycolysis to lactate production from [^{13}C]glucose. D-Ribose from RNA (ribose) was obtained as follows: cell pellets or tissue fragments were homogenized with the TRIzol reagent; RNA in the aqueous phase was hydrolyzed with 2 N HCl followed by neutralization; free ribose was purified by ion-exchange chromatography; purified ribose was derivatized to the aldonitrile acetate form by treatment with hydroxylamine hydrochloride in pyridine (*e.g.* 100 °C, 1 h) and acetic anhydride (*e.g.* 100 °C, 0.5 h) (25). [$^{12/13}$C]Ribose isotopomers were monitored by GC-MS at the ion clusters at *m/z* 242 and *m/z* 217 in the EI spectrum (carbons 1–4 and 3–5, respectively, of derivatized ribose). Together, these data were used to determine the relative contributions of the oxidative and nonoxidative PPC to ribose production from [^{13}C]glucose. For example, data for ribose with ^{13}C at the first carbon (ribose) position (*m/z* 242 C_1–C_4; M_1; using [$^{13}C_2$]glucose) was used to determine the fraction of ribose derived from [^{13}C]glucose in the oxidative PPC, initially catalyzed by glucose-6-phosphate dehydrogenase; data for ribose with ^{13}C at the first two carbon positions (*m/z* 242 C_1–C_4; M_2; using [$^{13}C_2$]glucose or using [$^{13}C_6$]glucose) was used to determine the fraction of ribose derived from [^{13}C]glucose in the nonoxidative PPC, catalyzed by transketolase; data for ribose with ^{13}C at the fourth and fifth carbon positions (*m/z* 217 C_3–C_5; M_2; using [$^{13}C_2$]glucose) was used to determine the fraction of ribose derived from [^{13}C]glucose by triose recycling and catalyzed by transketolase and transaldolase (24–26). Fatty acids (mainly C_{16} fatty acids/palmitate; palmitate below) were obtained from cell pellets by saponification with 30% KOH and 100% ethanol, followed by extraction with petroleum ether. Fatty acids were obtained from TRIzol homogenates of tissue fragments by chloroform extraction, saponification of the phenol/chloroform layer over 3 h with 0.6 ml of 15% KOH and 50% ethanol, and extraction with petroleum ether (*e.g.* three extractions, 5 ml/extraction). Extracted fatty acids were converted to the methyl esters by using 0.5 N methanolic HCl. Derivatized [$^{12/13}$C]palmitate isotopomers were monitored by GC-MS at the ion cluster at *m/z* 270 in the EI spectrum to determine the fraction of palmitate synthesized from [^{13}C]glucose or the fraction of acetyl units derived from [^{13}C]glucose in newly synthesized palmitate (25, 26).

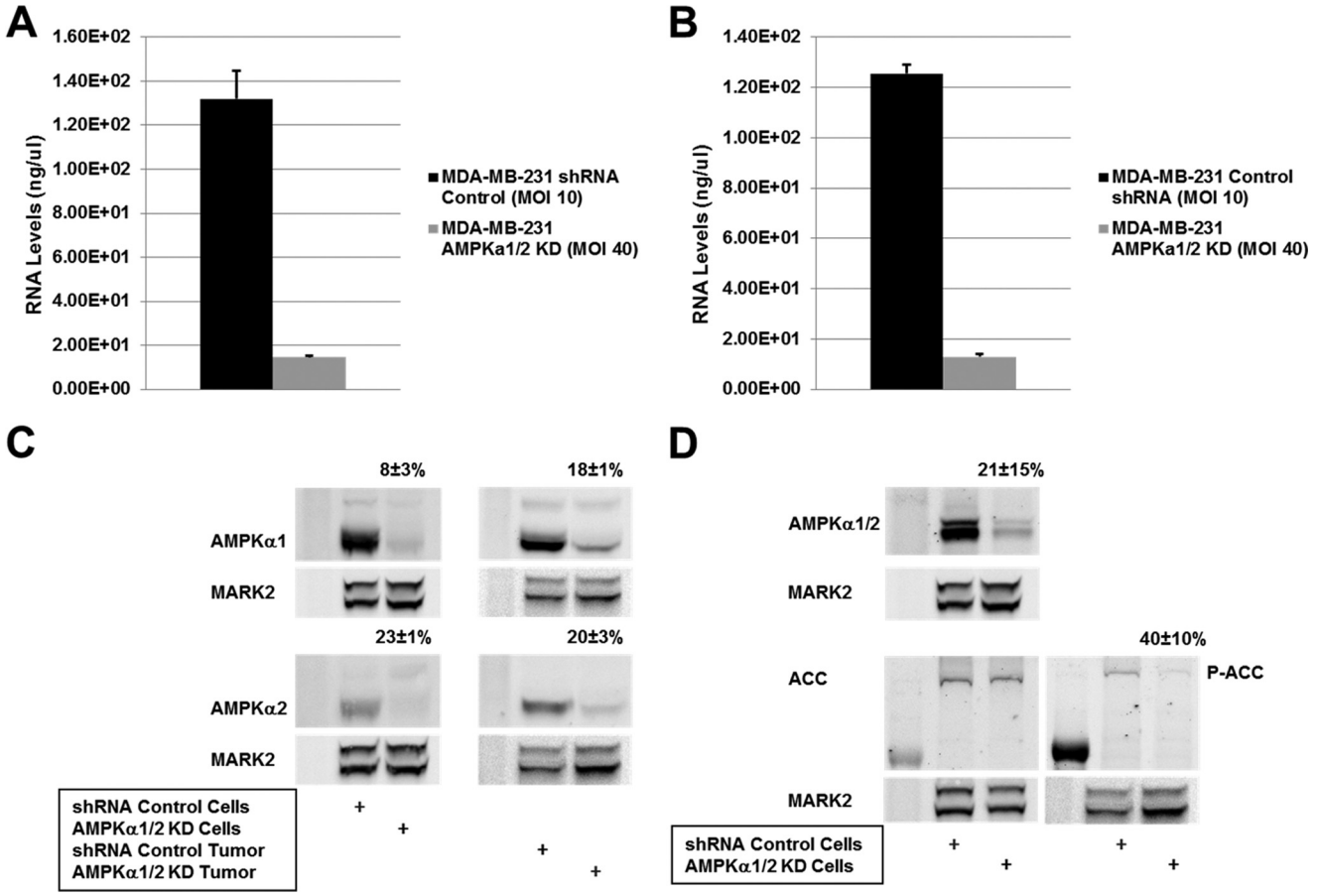

FIGURE 1. *A* and *B,* transcript levels of AMPKα1 (*PRKAA1*) and AMPKα2 (*PRKAA2*) in shRNA control and AMPKα1/2 KD MDA-MB-231 cells. Numerical values refer to % (KD Signal/Control Signal) $\pm$ % combined S.D. ($n = 2$ replicates). *C,* AMPKα1 and AMPKα2 protein levels in shRNA control and AMPKα1/2 KD MDA-MB-231 cells. Numerical values refer to % (normalized KD signal/normalized control signal) $\pm$ % combined S.D. ($n = 2$ replicates). AMPKα signals were normalized to the corresponding MARK2 signals (signals are intensity values (thousand pixels) obtained by image analysis). *D,* total AMPKα (AMPKα1/2), ACC1, and phospho-Ser-79 ACC1 (P-ACC1) protein levels in shRNA control and AMPKα1/2 KD MDA-MB-231 cells. Numerical values refer to % (normalized KD signal/normalized control signal) $\pm$ % combined S.D. ($n = 2$, replicates). AMPKα signals were normalized to the corresponding MARK2 signals (signals are intensity values (thousand pixels) obtained by image analysis).

Mass spectral data for the various metabolites were acquired with an Agilent HP 6890N gas chromatograph connected to a HP5975N mass selective detector (Agilent Technologies, Santa Clara, CA). An Agilent J&W Scientific HP-5-ms column (30 m in length; 250 μm in diameter; 0.25-μm film thickness; Part 19091S-433) was used for glucose, lactate, and ribose analysis. An Agilent J&W DB-23 column (60 m in length; 250 μm in diameter; 0.15 μm film thickness; Part 122-2361) was used for CO_2 and fatty acid analysis. Helium (>99.99% purity) and methane (>99.99% purity; Praxair, Danbury, CT) were used as gases for the EI and chemical ionization analysis modes, respectively. Samples were injected directly into the heated (250 °C) and pressurized inlet interface; examples of instrument settings for the metabolites are given in Refs. 24, 27.

Data Analysis and Statistical Methods for Metabolic Profiling—GC-MS analyses involved consecutive automatic injections of samples (1 μl); the mass spectral data were considered acceptable if the standard sample deviations for peak intensities from the repeated injections were <1% of the normalized peak intensities. Isotopomer peak data were obtained from three consecutive manual integrations of background-subtracted spectra containing overlapping isotopomer peaks, as displayed in the total ion chromatogram window using GC-MS analytical software (ChemStation, Agilent). Statistical analyses of control and experimental samples were performed using an unpaired heteroscedastic, two-tailed independent sample *t* test with 95% confidence intervals; $p < 0.05$ was considered to indicate significant differences in glucose carbon metabolism between shRNA control and AMPKα1/2 KD cells.

RESULTS

AMPK Supports the Growth of Aggressive Orthotopic Human Breast Tumor Xenografts—We achieved ≥80% KD of the expression of the AMPKα1/2 mRNAs (*PRKAA1/2*) in MDA-MB-231 cells infected with lentivirus particles encoding specifically targeted shRNAs (Fig. 1, *A* and *B*); control cells were infected with a lentivirus preparation encoding a scrambled shRNA. Fig. 1*C* shows a similar KD of the expression of AMPKα1 and -α2 protein in the MDA-MB-231 cell lines (shRNA control and AMPKα1/2 KD cells). The greater expression of AMPKα1 compared with -α2 proteins evident in Fig. 1*C* is consistent with genomic data for MDA-MB-231 cells; the gene copy numbers for chromosome 5 (the *PRKAA1* locus) and chromosome 1 (the *PRKAA2* locus) are 4*n* and 2*n*, respectively (COSMIC Database, Cell Lines Project). We have routinely detected relatively greater levels of AMPKα1 compared with

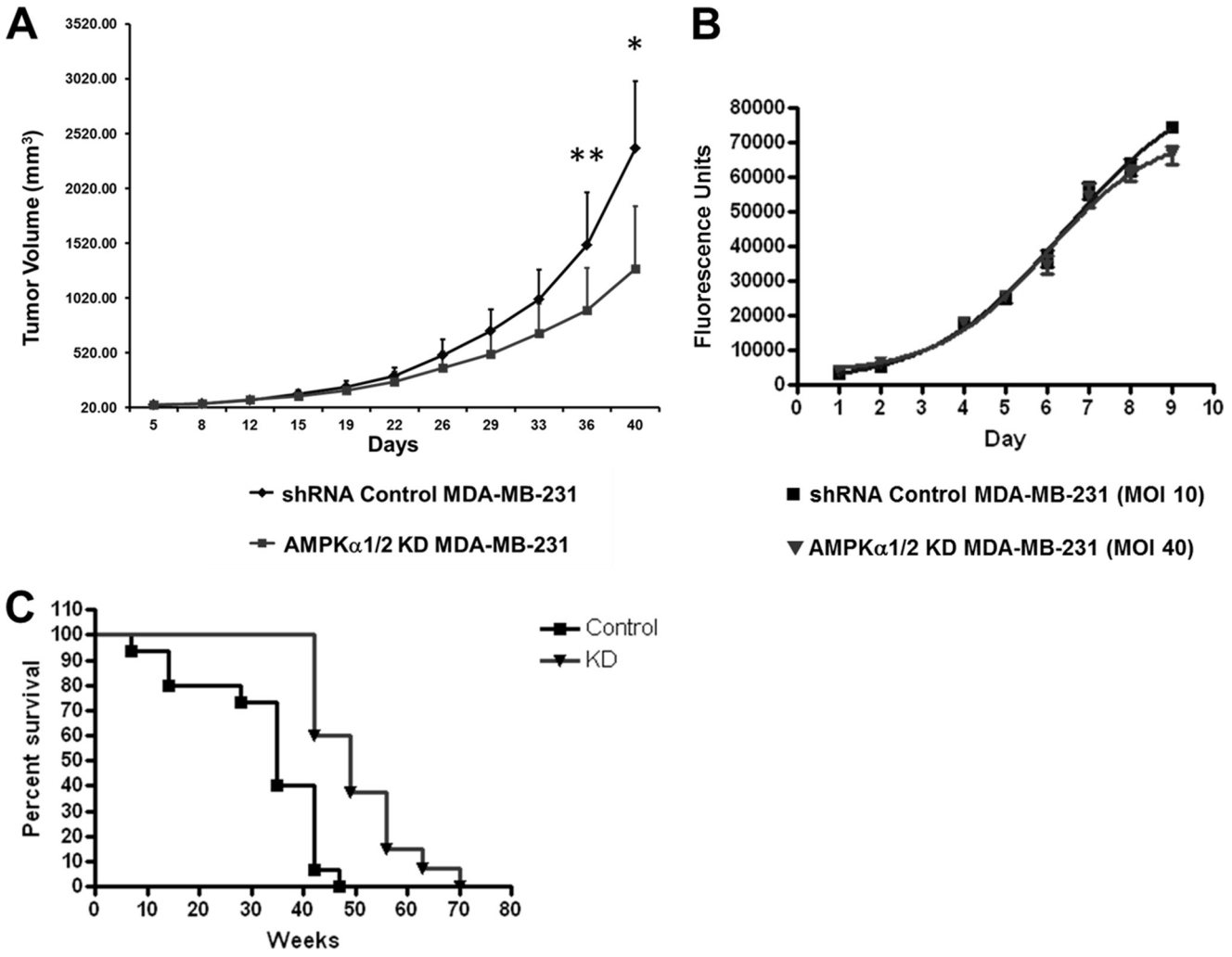

FIGURE 2. *A,* effect of an AMPKα1/2 KD on the growth of orthotopic MDA-MB-231 xenografts in nude mice (10 implanted mice/group). Mean tumor volume data were analyzed by one-way analysis of variance ($p < 0.0001$). The *asterisks* refer to *p* values for statistically significant differences ($p < 0.05$; Tukey-Kramer test) at the indicated days of tumor growth: *, day 40, $p < 0.001$; **, day 36, $p < 0.05$ (shRNA control group, *top curve/diamonds*; AMPKα1/2 KD group, *bottom curve/squares*). *Error bars,* ±S.D. *B, in vitro* proliferation/survival curves for shRNA control and AMPKα1/2 KD MDA-MB-231 cells obtained by using an Alamar Blue proliferation/viability assay. Raw fluorescence data were fitted by nonlinear regression to a sigmoidal growth equation. *Error bars,* ±S.D. ($n = 3$ replicates). *C,* survival curves from a lung colonization assay experiment involving control and AMPKα1/2 KD MDA-MB-231 cells. MDA-MB-231 cells were injected into the tail vein of beige-nude mice (2×10^6 cells/injection; 15 mice/group). Survival was determined by the Kaplan-Meier method ($p < 0.0001$ for median survival). *Top curve* (*triangles*), AMPKα1/2 KD group; *bottom curve* (*squares*), shRNA control group.

-α2 on immunoblots of total protein from human cell lines using the antibodies described under "Experimental Procedures." AMPK activity is commonly monitored by immunological detection of specific phosphorylation of its substrate acetyl-CoA carboxylase 1 (ACC1; Ser-79 in human cells) (9, 28); AMPKα1/2 KD significantly attenuated this phosphorylation in MDA-MB-231 cells (*P-ACC,* Fig. 1*D*). More directly, as discussed below, *in vitro* metabolic profiling with a [^{13}C]glucose tracer showed that AMPKα1/2 KD in MDA-MB-231 cells altered fatty acid synthesis in a way that is consistent with AMPK-dependent phosphorylation of ACC1. Together, these data demonstrate that we had achieved a substantial and functional KD of AMPK activity in MDA-MB-231 cells using the shRNA lentiviral preparation.

To determine whether AMPK is important for the growth of MDA-MB-231 tumors, we used the shRNA control and AMPKα1/2 KD MDA-MB-231 cells to initiate orthotopic tumors in nude mice and monitored tumor growth for 6 weeks. Fig. 2*A* shows growth curves constructed from the mean tumor volumes from this study as follows: tumors in the AMPKα1/2 KD group became significantly smaller than tumors in the shRNA control group by day 36, and by day 40 this difference was substantial (control tumors, 2,385 ± 613 mm^3; AMPKα1/2 KD tumors, 1,287 ± 572 mm^3; ±S.D., $p < 0.001$). Fig. 1*C* shows an example of AMPKα1 and -α2 protein expression in lysates of shRNA control and AMPKα1/2 KD tumors; immunoblot analysis of randomly selected shRNA control and AMPKα1/2 KD tumors from the study (four tumors/group) indicated that ≥70% KD of AMPKα1/2 expression was retained in the AMPKα1/2 KD compared with the shRNA control groups (Fig. 2*A*). In contrast to the inhibitory effect of AMPKα1/2 KD on the growth of orthotopic MDA-MB-231 tumors, Fig. 2*B* shows that there was no significant difference in the proliferation or survival of the same shRNA control and AMPKα1/2 KD cells when they were cultured in nutrient-rich medium (complete medium under normoxia (5% CO_2 + air)).

Fig. 2*C* shows Kaplan-Meier survival curves derived from a tumor colonization assay study (17) in which the shRNA control and AMPKα1/2 KD MDA-MB-231 cells were injected i.v. into beige-nude mice to establish tumors in lung (tumor burden was monitored by bioluminescence imaging; see "Experimental Procedures"). We note that the rapid growth of the orthotopic MDA-MB-231 tumors precluded the use of bioluminescence imaging to evaluate whether AMPK activity influenced the dissemination or local invasiveness of MDA-MB-231 cells in nude mice (spontaneous metastasis) (13). Fig. 2*C* shows that there were survivors in the shRNA control and AMPKα1/2 KD groups until days 49 and 70, respectively (mice were sacrificed during the study in accordance with IACUC guidelines). The *curves* in Fig. 2*C* are significantly different ($p < 0.0001$, log-rank test) with median survival rates of 35 days (shRNA control group) and 49 days (AMPKα1/2 KD group). Thus, MDA-MB-231 tumor burden in mouse lung tissue caused substantial pathology or morbidity more rapidly in the shRNA control than in the AMPKα1/2 KD group. This study indicates that the effect of AMPKα1/2 KD on the growth or development of MDA-MB-231 tumors does not require an orthotopic tissue microenvironment. The study also demonstrates that the use of Matrigel to initiate MDA-MB-231 tumors is not essential to reveal an AMPK-dependent effect(s) on the tumor biology of MDA-MB-231 cells in nude mice.

To test whether the AMPK-dependent growth defect observed using MDA-MB-231 tumors could be reproduced with a different TN human breast cancer cell line, we infected DU4475 cells with the same lentiviral preparations that were used to generate the shRNA control and AMPKα1/2 KD MDA-MB-231 cells, and we used the shRNA control and AMPKα1/2 KD DU4475 cells to generate orthotopic tumors in nude mice ($n = 10$ mice/group). Again, the AMPKα1/2 KD tumors showed a significant and substantial growth defect compared with the control tumors (*e.g.* mean tumor volumes on day 21: shRNA control group, 1271 ± 268 mm^3; AMPKα1/2 KD group, 552 ± 352 mm^3; $\pm$S.D.; $p < 0.001$). The study was terminated on day 21 in accordance with IACUC guidelines. As we found with the shRNA control and AMPKα1/2 KD MDA-MB-231 cells, there was no significant difference in the proliferation/survival of the shRNA control and AMPKα1/2 KD DU4475 cells when they were cultured in nutrient-rich medium (data not shown).

As mentioned in the Introduction, a major consideration of our rationale for using MDA-MB-231 cells to investigate the importance of AMPK for experimental breast tumor growth was that these cells have a Warburg effect (12), which is a common metabolic phenotype of human tumor cells, including breast cancer cells (1, 3). Therefore, we evaluated the effect of AMPKα1/2 KD on the core glucose metabolism of MDA-MB-231 cells both in cell culture and in orthotopic tumors.

AMPK Regulates Core Glucose Metabolism in MDA-MB-231 Cells—To investigate whether AMPK contributes to the Warburg effect in MDA-MB-231 cells, we used stable isotope-based metabolic profiling (metabolic profiling) (23, 26) with [$^{13}C_2$]- or [$^{13}C_6$]glucose tracers to investigate the effect of AMPKα1/2 KD on the core glucose metabolism of these cells both *in vitro* (cell culture) and *in vivo* (orthotopic tumors). Specifically, we used the distribution of ^{13}C atoms from [^{13}C]glucose to trace carbon flow from glucose through glycolysis, the PPC, the TCA cycle, and C_{16} fatty acid (palmitate) synthesis.

As detailed under "Experimental Procedures," to investigate glucose metabolism in cultures of shRNA control and AMPKα1/2 KD MDA-MB-231 cells, cells were incubated at 37 °C for 48 h (steady-state labeling) in medium containing either 25 or 1 mM total glucose (containing [$^{13}C_2$]glucose). MDA-MB-231 cells cultured in 1 mM glucose were used as a control for the effect of the proliferative state on glucose metabolism. Fig. 3*A* shows that the proliferation of both shRNA control and AMPKα1/2 KD MDA-MB-231 cells was attenuated in 1 mM compared with 25 mM glucose-containing medium. During the 48-h incubation time, there was no significant difference between the shRNA control and AMPKα1/2 KD cells in the uptake of [$^{12/13}$C]glucose from the medium (data not shown); in support of this finding, measurements of steady-state uptake of glucose by subconfluent shRNA control and AMPKα1/2 KD MDA-MB-231 cells incubated with 2-[1,2-^{3}H]deoxy-D-glucose over a 5-min incubation time showed no statistically significant difference in glucose uptake (Fig. 3*B*). Thus, differences in glucose metabolism detected by metabolic profiling of the shRNA control and AMPKα1/2 KD cells (described below) cannot be attributed to differences in glucose uptake from the medium over 48 h of incubation.

Fig. 4*B* shows that the complete oxidation of glucose to CO_2 (in the PPC and the TCA cycle) in MDA-MB-231 cells was increased by AMPKα1/2 KD, as indicated by the increased ^{13}C/^{12}C ratio in $^{12/13}CO_2$ ($\delta^{13}CO_2$) obtained from the high glucose medium (25 mM glucose) of AMPKα1/2 KD cells compared with the high glucose medium (25 mM glucose) of shRNA control cells. This finding indicates that AMPK is important for the anabolic (anaplerotic) compared with the catabolic (oxidative) utilization of glucose by MDA-MB-231 cells in high glucose medium. Fig. 4*C* shows that the release of [$^{12/13}$C]lactate (total lactate) from AMPKα1/2 KD cells was significantly decreased compared with that from shRNA control cells in high glucose medium (total integrated peak area/volume of medium). There were no significant differences in the relative contributions of (aerobic) glycolysis and the PPC to lactate production for either the AMPKα1/2 KD or the shRNA control cells, as indicated by the M1, M2, and M3 metabolites at *m/z* 328 (data not shown). These findings indicate that AMPK regulates the utilization of glucose by both glycolysis and the PPC pathways in MDA-MB-231 cells cultured in high glucose medium. Both cell lines produced less lactate in low glucose (1 mM glucose) medium compared with high glucose medium, which is consistent with the lower rates of proliferation of the cells in low glucose medium (Fig. 3*A*).

Fig. 4, *D* and *E*, shows that the utilization of glucose for ribose synthesis did not differ between the AMPKα1/2 KD and shRNA control cells in high or low glucose medium; production of ^{13}C-labeled ribose from all pathways (Fig. 4, *D*, PPC, and *E*, triose recycling) as a percentage of total [^{12,13}C]ribose was not significantly different between the shRNA control and AMPKα1/2 KD cells. In high glucose medium, however, AMPKα1/2 KD cells preferentially synthesized ribose through the oxidative rather than the nonoxidative PPC (Fig. 4, *F* and *G*,

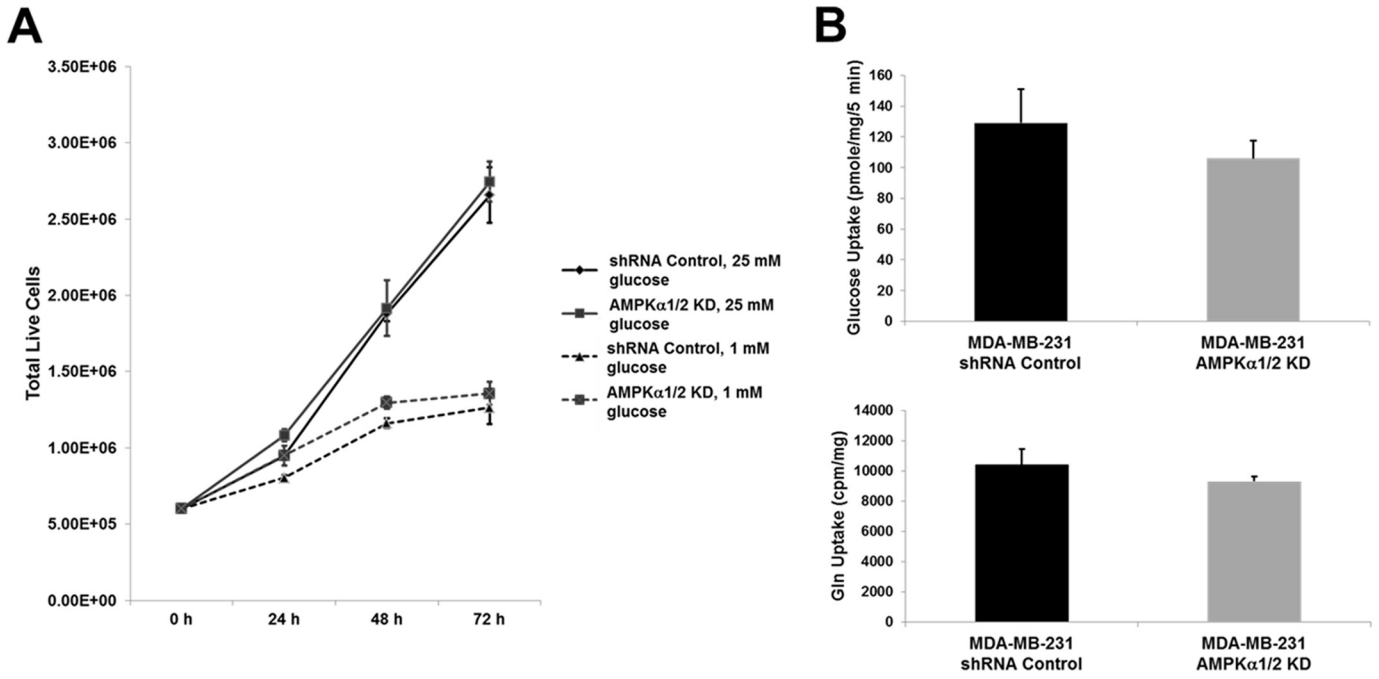

FIGURE 3. *A, in vitro* growth curves for shRNA control and AMPKα1/2 KD MDA-MB-231 cells cultured in high and low glucose-containing medium (25 or 1 mM glucose in DMEM + 10% FBS; data obtained by cell counting). *Error bars,* ±S.D. ($n = 3$ replicates). *Top curves* (*solid lines*), 25 mM glucose; *bottom curves* (*broken lines*), 1 mM glucose. *B,* effect of AMPKα1/2 KD on the uptake of glucose (*top*) and glutamine (*bottom*) by MDA-MB-231 cells cultured under normoxia (5% CO_2 + air). Cells were given 2-deoxy-D-[2,6-^{3}H]glucose or L-[3,4-^{3}H]glutamine for 5 min (see under "Experimental Procedures" for details). Glucose uptake: shRNA control cells, 129 ± 22 pmol/mg total protein/5 min; AMPKα1/2 KD cells, 106 ± 11 pmol/mg total protein/5 min; ±S.D., $n = 3$. Glutamine uptake: shRNA control cells, 10,411 ± 1,034 cpm/mg total protein/5 min; AMPKα1/2 KD cells, 9320 ± 314 pmol/mg total protein/5 min; ±S.D., $n = 3$.

respectively; M_1 and M_2 as percentages of the [^{13}C]ribose (C_1-C_4) fraction), compared with shRNA control cells. Because the oxidative PPC is a major source of cellular NADPH, which is directly synthesized from $NADP^+$ by glucose-6-phosphate dehydrogenase (3), this finding indirectly indicates that proliferative AMPKα1/2 KD cells synthesized more NADPH than proliferative shRNA control cells in high glucose medium. In this context, in high glucose medium AMPKα1/2 KD cells also produced more palmitate from glucose than shRNA control cells (Fig. 4*H*, ^{13}C-labeled palmitate from all pathways as a percentage of total [^{12,13}C]palmitate) using acetyl-CoA (Fig. 4*I*, [^{13}C]acetate as a percentage of total palmitate). Cytoplasmic acetyl-CoA, which is derived from the TCA cycle by citrate shuttling, is converted by acetyl-CoA carboxylase to malonyl-CoA; malonyl-CoA is used for the reductive (NADPH-dependent) synthesis of palmitate and longer chain fatty acids by fatty-acid synthase (2). The finding that AMPKα1/2 KD cells had increased synthesis of palmitate compared with shRNA control cells (in high glucose medium) is consistent with the established biochemistry of AMPK; AMPK-dependent phosphorylation of ACC1 inhibits the production of malonyl-CoA, which decreases the synthesis of long chain fatty acids by fatty-acid synthase (6, 7). Thus, all other things being equal, the increased synthesis of palmitate in AMPKα1/2 KD compared with shRNA control MDA-MB-231 cells is a predictable consequence of inhibition of AMPK activity.

The differences in glucose utilization between shRNA control and AMPKα1/2 KD MDA-MB-231 cells described above were not evident in measurements of oxygen consumption rates (respiration) and proton production rates (medium acidification) under similar culture conditions (Fig. 5). A possible explanation for the apparent discrepancy between the results of [^{13}C]lactate analysis (Fig. 4*C*) and the medium acidification results (Fig. 5*B*) is that both shRNA and AMPKα1/2 KD MDA-MB-231 cells could produce lactate from glutamine as well as from glucose catabolism (1): indeed, Fig. 3*B* shows that both cell lines acquired glutamine from complete medium with indistinguishable kinetics.

AMPK Regulates Core Glucose Metabolism in Orthotopic Tumors Prepared from MDA-MB-231 Cells—To investigate the effect of AMPKα1/2 KD on core glucose metabolism in MDA-MB-231 cells *in vivo*, we performed metabolic profiling with [$^{13}C_6$]glucose in a second orthotopic tumor xenograft study using the shRNA control and AMPKα1/2 KD MDA-MB-231 cell lines. Fig. 6*B* shows tumor growth curves from this study; tumors in the AMPKα1/2 KD group became significantly smaller than tumors in the shRNA control group (*e.g.* day 21; shRNA control tumors, 405 ± 105 mm^3; AMPKα1/2 KD tumors, 296 ± 51 mm^3; ±S.D.; $p < 0.001$), in agreement with the growth results from the first orthotopic tumor study shown in Fig. 2*A*. As described under "Experimental Procedures," groups of mice with shRNA control or AMPKα1/2 tumors were sacrificed at 30, 60, or 90 min after injection of the [$^{13}C_6$]glucose tracer to evaluate core glucose metabolism in tumors and selected organs (liver and pancreas) from each mouse. Data obtained from the 30-min sacrifice time effectively represent the response of the various tissues to a glucose challenge. We note that the brief ^{13}C-labeling times (30–90 min) used here enabled analysis of core glucose metabolism in shRNA control and AMPKα1/2 KD tissues independently of net tumor growth rates.

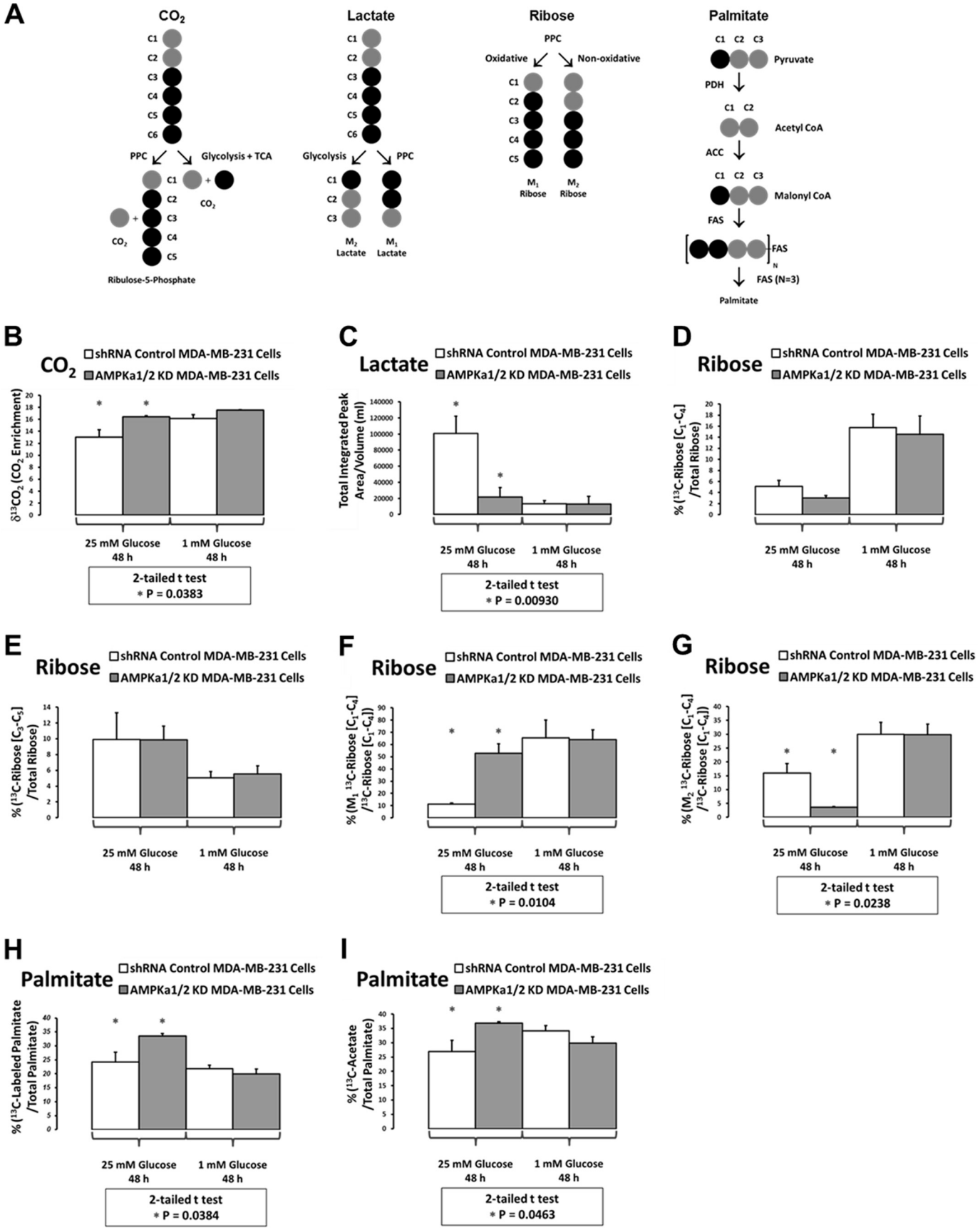
A
CO2
Lactate
Ribose
Palmitate
PPC
Glycolysis + TCA
Glycolysis
Oxidative
Non-oxidative
Pyruvate
PDH
Acetyl CoA
ACC
Malonyl CoA
FAS
FAS (N=3)
Ribulose-5-Phosphate
B
CO2
shRNA Control MDA-MB-231 Cells
AMPKa1/2 KD MDA-MB-231 Cells
δ13CO2 (CO2 Enrichment)
25 mM Glucose 48 h
1 mM Glucose 48 h
2-tailed t test
* P = 0.0383
C
Lactate
Total Integrated Peak Area/Volume (ml)
* P = 0.00930
D
Ribose
% (13C-Ribose [C1-C4] /Total Ribose)
E
% (13C-Ribose [C3-C5] /Total Ribose)
F
% (M1 13C-Ribose [C1-C4] /13C-Ribose [C1-C4])
* P = 0.0104
G
% (M2 13C-Ribose [C1-C4] /13C-Ribose [C1-C4])
* P = 0.0238
H
Palmitate
% (13C-Labeled Palmitate /Total Palmitate)
* P = 0.0384
I
% (13C-Acetate /Total Palmitate)
* P = 0.0463

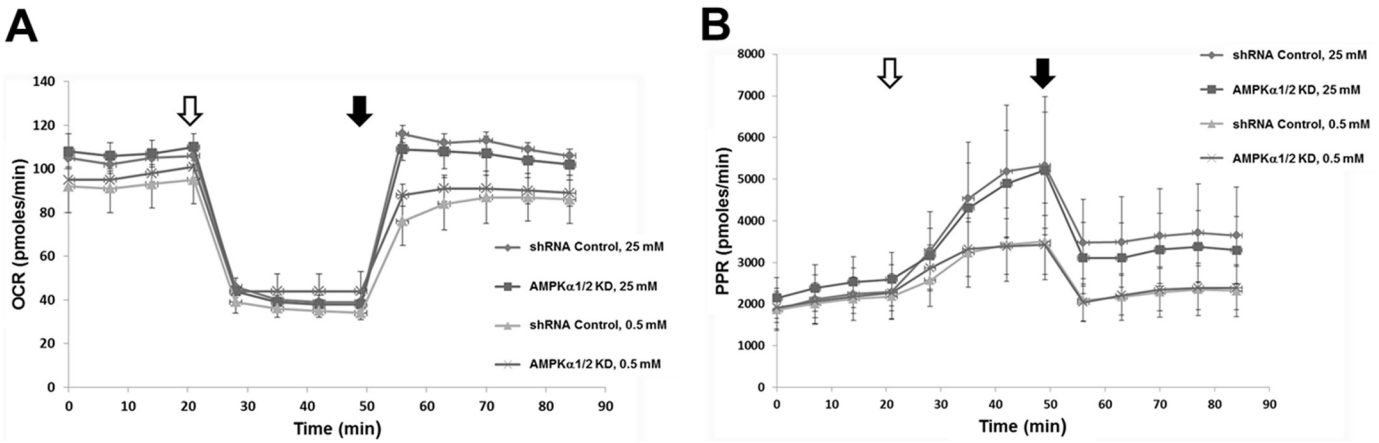

FIGURE 5. **Effect of AMPKα1/2 KD on the oxygen consumption rate (*OCR*) (*A*) and proton production rate (*PPR*) (*B*) of MDA-MB-231 cells cultured under normoxia (5% CO_2 + air).** *Open arrow*, addition of the ATP synthase inhibitor oligomycin to inhibit oxidative phosphorylation. *Closed arrow*, addition of the uncoupling agent/protonophore (carbonyl cyanide *m*-chlorophenyl hydrazone) to uncouple the respiratory chain from ATP synthesis. *Error bars,* ±S.D.

Fig. 6*C* shows that the complete oxidation of glucose to CO_2 (in the PPC and the TCA cycle) in tumor tissue was decreased by AMPKα1/2 KD, as indicated by the decreased $^{13}C/^{12}C$ ratio in $^{12/13}CO_2$ ($\delta^{13}CO_2$) from AMPKα1/2 KD compared with shRNA control tumors. This finding contrasts with that obtained for CO_2 production with cultures of the shRNA control and AMPKα1/2 KD MDA-MB-231 cells by *in vitro* metabolic profiling (Fig. 4*B*). Fig. 6*D* shows that [$^{12/13}$C]lactate (total lactate) in AMPKα1/2 KD tumors was decreased compared with total lactate from shRNA control tumors (total integrated peak area/tissue weight). On glucose challenge (30-min sacrifice time), AMPKα1/2 KD tumors produced less ^{13}C-labeled lactate from all pathways (glycolysis, PPC + glycolysis) than shRNA control tumors (Fig. 6*E*; ^{13}C-labeled lactate from all pathways as a percentage of total [$^{12/13}$C]lactate). The decreased lactate production found in AMPKα1/2 KD compared with shRNA control MDA-MB-231 tumors was also found with the same cell lines by *in vitro* metabolic profiling (Fig. 4*C*). Compared with shRNA control tumors, on glucose challenge AMPKα1/2 KD tumors produced relatively more lactate from the oxidative PPC + glycolysis than directly from glycolysis (Fig. 6*F*; M_2 [$^{13}C_2$]lactate/M_3 [$^{13}C_3$]lactate) (23). Fig. 6*G* shows that total RNA ribose ([$^{12/13}$C]ribose, total ribose) from AMPKα1/2 KD tumors was decreased compared with total ribose from shRNA control tumors (total integrated peak area/tissue weight). Moreover, synthesis of ribose through the nonoxidative PPC was decreased in the AMPKα1/2 KD compared with the shRNA control tumors (Fig. 6*H*; M_2 as a percentage of the [^{13}C]ribose [C_1–C_4] fraction). This finding suggests that AMPK supports the synthesis of ribose through the nonoxidative compared with the oxidative PPC in MDA-MB-231 tumors, although the amount of total ribose was less in AMPKα1/2 KD compared with shRNA control MDA-MB-231 tumors (Fig. 6*G*). The relatively decreased synthesis of [$'^3$C]ribose in the nonoxidative PPC found in AMPKα1/2 KD compared with shRNA control tumors was found with the same cell lines by *in vitro* metabolic profiling (Fig. 4*G*). AMPKα1/2 KD tumors did not detectably synthesize an increased amount of palmitate from [$^{12/13}$C]glucose during the times used for the metabolic profiling study (30–90 min), unlike shRNA control tumors (Fig. 6*I*, total integrated peak area/tissue weight; Fig. 6*J*, [^{13}C]palmitate as a percentage of total palmitate). Fig. 6*K* shows that on glucose challenge shRNA control but not AMPKα1/2 KD tumors synthesized new palmitate from acetyl-CoA ([^{13}C]acetate as a percentage of total palmitate). Together, the findings shown in Fig. 6, *I–K,* indicate that compared with shRNA control MDA-MB-231 tumors, AMPKα1/2 KD MDA-MB-231 tumors had lower rates of palmitate synthesis from [^{13}C]acetyl-CoA, in contrast to cultures of the same cell lines in conventional medium (Fig. 4, *H* and *I*; 48-h ^{13}C-labeling time). As with ribose synthesis, the decreased amount of palmitate synthesis in AMPKα1/2 KD compared with shRNA control tumors correlated with the relatively decreased growth state of the AMPKα1/2 KD tumors (Fig. 6*B*).

Orthotopic Tumors Prepared from shRNA Control and AMPKα1/2 KD MDA-MB-231 Cells Alter Host Glucose Metabolism—The incorporation of ^{13}C atoms from a glucose tracer within RNA ribose can be used as an end point to evaluate the consequences of a metabolic perturbation such as tumor burden on host glucose homeostasis (29). Fig. 7*A* shows that glucose homeostasis was altered in both pancreas and liver of mice with AMPKα1/2 KD tumors; the production of RNA ribose in both organs was significantly and substantially increased in mice with shRNA control compared with AMPKα1/2 KD tumors. Moreover, compared with liver in mice with shRNA control tumors, liver in mice with AMPKα1/2 KD tumors produced relatively more lactate from the oxidative PPC + glycolysis than from glycolysis (Fig. 7*B*; M_2

FIGURE 4. **Metabolic profiling of shRNA control and AMPKα1/2 KD MDA-MB-231 cells cultured with a D-[1,2-$^{13}C_2$]glucose tracer in high and low glucose-containing medium (25 or 1 mM glucose in DMEM +10% FBS).** Histograms show the effect of AMPKα1/2 KD on glucose metabolism through the following pathways. *A,* ^{13}C-labeling patterns of selected molecules of core glucose metabolism evaluated using [$^{13}C_2$]glucose as a tracer. *B,* oxidation to CO_2 in the PPC and the TCA cycle; *C,* production of lactate by aerobic glycolysis and the PPC; *D–F,* production of RNA ribose by triose recycling (*D*), the PPC (*E*), the oxidative PPC (*F*), and the nonoxidative PPC (*G*); production of palmitate from all pathways (*H*) and from acetyl-CoA from the TCA cycle (*I*). *Error bars,* ±S.D. (n = 3 plates/cell line).

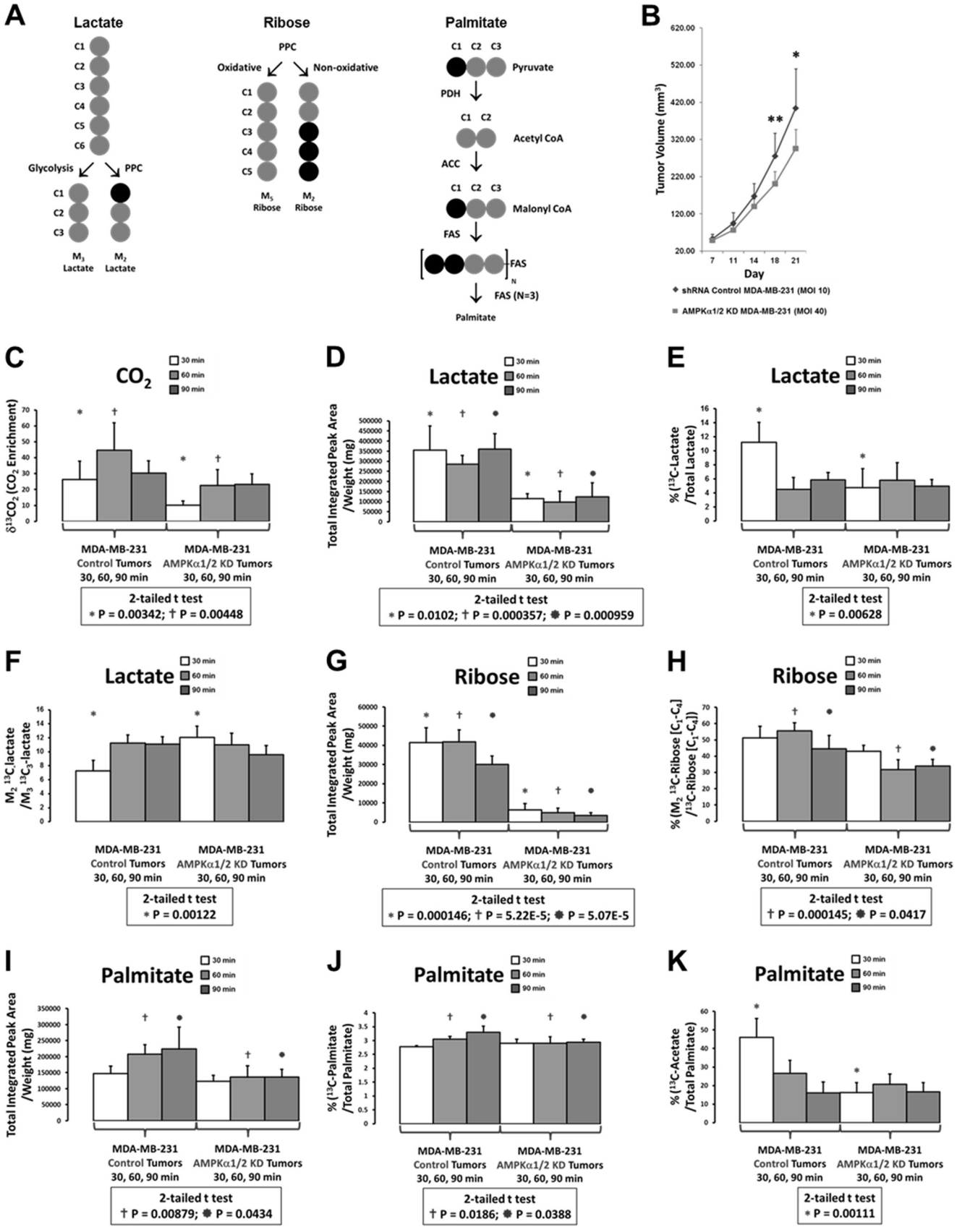
A
Lactate
C1
C2
C3
C4
C5
C6
Glycolysis
PPC
C1
C2
C3
M3 Lactate
M2 Lactate
Ribose
PPC
Oxidative
Non-oxidative
C1
C2
C3
C4
C5
M5 Ribose
M2 Ribose
Palmitate
C1 C2 C3
Pyruvate
PDH
C1 C2
Acetyl CoA
ACC
C1 C2 C3
Malonyl CoA
FAS
FAS
N
FAS (N=3)
Palmitate
B
Tumor Volume (mm3)
620.00
520.00
420.00
320.00
220.00
120.00
20.00
7 11 14 18 21
Day
shRNA Control MDA-MB-231 (MOI 10)
AMPKα1/2 KD MDA-MB-231 (MOI 40)
C
CO2
30 min
60 min
90 min
δ13CO2 (CO2 Enrichment)
MDA-MB-231 Control Tumors 30, 60, 90 min
MDA-MB-231 AMPKα1/2 KD Tumors 30, 60, 90 min
2-tailed t test
* P = 0.00342; † P = 0.00448
D
Lactate
Total Integrated Peak Area /Weight (mg)
2-tailed t test
* P = 0.0102; † P = 0.000357; ● P = 0.000959
E
Lactate
% (13C-Lactate /Total Lactate)
2-tailed t test
* P = 0.00628
F
Lactate
M2 13C-lactate /M3 13C3-lactate
2-tailed t test
* P = 0.00122
G
Ribose
Total Integrated Peak Area /Weight (mg)
2-tailed t test
* P = 0.000146; † P = 5.22E-5; ● P = 5.07E-5
H
Ribose
% (M2 13C-Ribose [C1-C4] /13C-Ribose [C1-C4])
2-tailed t test
† P = 0.000145; ● P = 0.0417
I
Palmitate
Total Integrated Peak Area /Weight (mg)
2-tailed t test
† P = 0.00879; ● P = 0.0434
J
Palmitate
% (13C-Palmitate /Total Palmitate)
2-tailed t test
† P = 0.0186; ● P = 0.0388
K
Palmitate
% (13C-Acetate /Total Palmitate)
2-tailed t test
* P = 0.00111

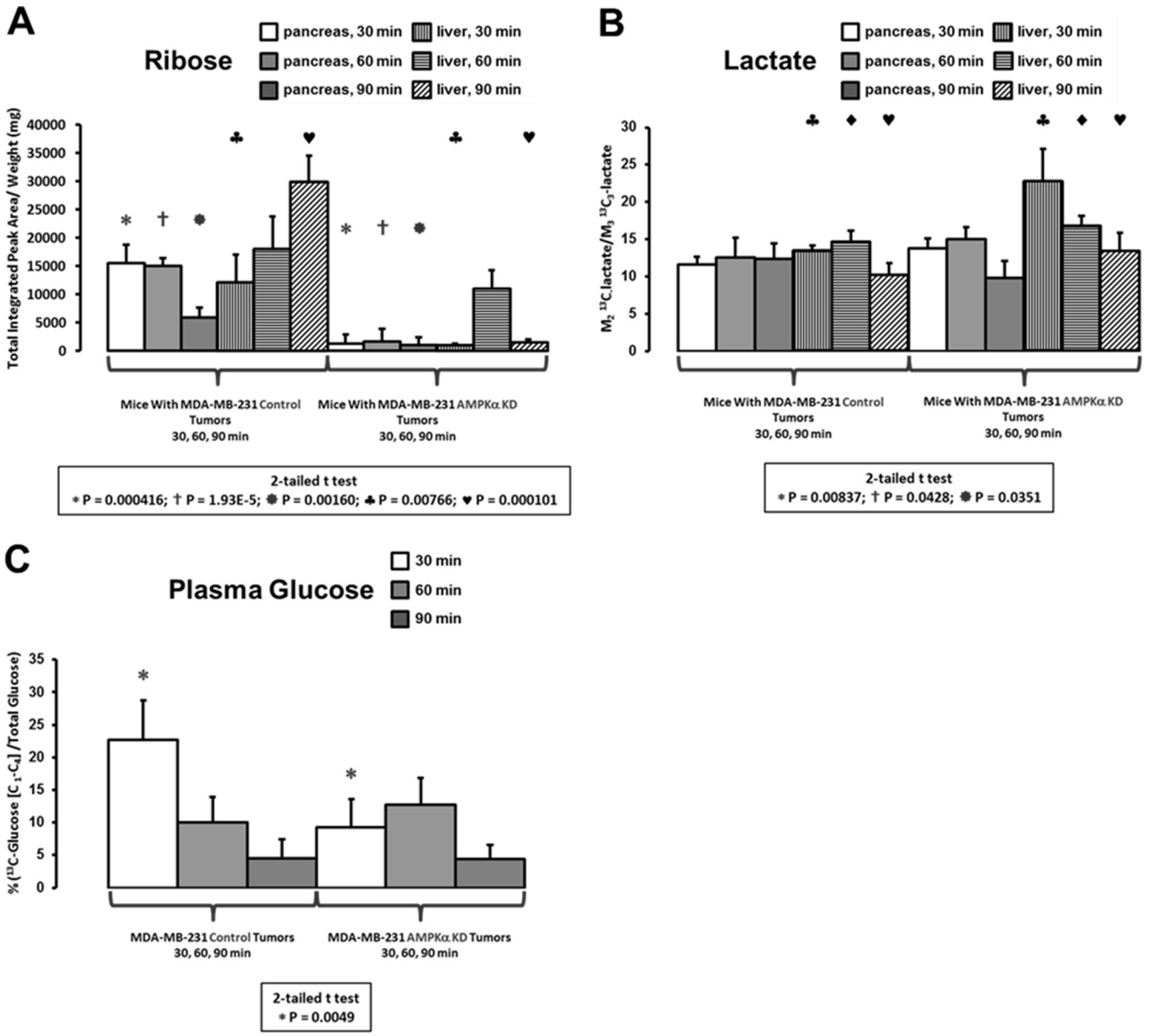

FIGURE 7. **Metabolic profiling of pancreas and liver from mice used for the study detailed in Fig. 6.** *Histograms* show the effect of AMPKα1/2 KD on glucose metabolism in pancreas and liver tissue through the following pathways: *A,* production of RNA ribose by all pathways; and *B,* production of lactate by the oxidative PPC relative to glycolysis. *C,* enrichment of ^{13}C from the D-[$^{13}C_6$]glucose tracer in plasma glucose. *Error bars,* ±S.D.

[$^{13}C_2$]lactate/M_3 [$^{13}C_3$]lactate). Together these findings indicate that orthotopic MDA-MB-231 tumor burden had systemic effects on normal tissue glucose homeostasis in the murine host and that AMPKα1/2 KD in MDA-MB-231 cells altered this homeostasis. Considering that MDA-MB-231 cells have a Warburg effect (12), it is conceivable that the high glucose demand of rapidly growing MDA-MB-231 tumors altered the availability of the plasma glucose pool for both the pancreas and liver in mice with shRNA control tumors. In fact, on glucose challenge (30-min time point) the level of ^{13}C-enriched plasma glucose (representing dilution by the pre-existing glucose pool and new synthesis by hepatic gluconeogenesis) was significantly lower in AMPKα1/2 KD compared with shRNA control tumors (Fig. 7*C*). This finding could be interpreted as the outcome of

FIGURE 6. **Metabolic profiling of shRNA control and AMPKα1/2 KD MDA-MB-231 orthotopic tumors with a D-[$^{13}C_6$]glucose tracer.** *A,* ^{13}C-labeling patterns of selected molecules of core glucose metabolism evaluated using [$^{13}C_6$]glucose as a tracer. *B,* growth curves for the orthotopic MDA-MB-231 tumors used for the study (30 implanted mice/group). Mean tumor volume data were analyzed by one-way analysis of variance ($p < 0.0001$). The *asterisks* refer to *p* values ($p < 0.05$; Tukey-Kramer test) for statistically significant differences in mean tumor volumes ($p < 0.050$) at the indicated days of tumor growth: *, day 21, $p < 0.001$; **, day 18, $p < 0.001$ (shRNA control group, *top curve/diamonds*; AMPKα1/2 KD group, *bottom curve/squares*). *Error bars,* ±S.D. Histograms show the effect of AMPKα1/2 KD on core glucose metabolism in tumor tissue (during ≤90 min; *left-to-right*, 30-, 60-, and 90-min observation times; five tumors/time) through the following pathways: *C,* oxidation to CO_2 in the PPC and the TCA cycle; *D* and *E,* production of lactate by glycolysis and the PPC; *F,* production of lactate by the oxidative PPC relative to glycolysis; production of RNA ribose by all pathways (*G*) and the nonoxidative PPC (*H*); production of palmitate from all pathways (*I* and *J*) and from acetyl-CoA from the TCA cycle (*K*). Tumor tissue and plasma samples were obtained on day 21 at 30-, 60-, and 90-min after i.p. injection of the tracer (15 mice from each group were used for metabolic profiling; 5 mice/time point; see "Experimental Procedures" for details). *Error bars,* ±S.D.

decreased intraperitoneal uptake of the [^{13}C]glucose tracer or increased dilution of the tracer with newly synthesized [$^{12}C_6$]glucose (or both), in mice with AMPKα1/2 KD compared with shRNA control tumors. The effect of AMPKα1/2 KD in MDA-MB-231 tumors on host glucose homeostasis is discussed further below.

DISCUSSION

A significant finding of this study is that AMPK supports the growth of experimental orthotopic tumors prepared from an aggressive human tumor cell line, MDA-MB-231 breast cancer cells, which have a TN classification (Fig. 2*A*) (10). In contrast to the positive effect of AMPK on the growth of MDA-MB-231 tumors, AMPK was dispensable for the proliferation or viability of the same cells in nutrient-rich (normal) culture medium (Fig. 2*B*). We observed essentially identical AMPK-dependent *in vitro* and *in vivo* phenotypes using DU4475 cells, another TN human breast cancer cell line (10, 30). These findings, which phenocopy our previous *in vivo* and *in vitro* findings using AMPKα1/2 KO *HRAS* G12V-transformed mouse embryo fibroblasts (8), suggest that the contribution of AMPK to the growth of an aggressive experimental solid tumor has a critical microenvironmental component. This idea is consistent with the established physiological model of AMPK function; in response to ATP depletion, AMPK acts to restore energy homeostasis by inhibiting ATP-consuming processes and stimulating ATP-generating processes (6, 7). Thus, stimulated AMPK activity within the metabolically stressed microenvironments that develop in rapidly growing solid tumors (2, 5) could confer an adaptive or pro-survival advantage on tumor cells subjected to severe ATP depletion (6).

We applied *in vitro* and *in vivo* metabolic profiling with [^{13}C]glucose tracers to investigate the importance of AMPK for regulating core glucose metabolism in the MDA-MB-231 cell line by comparing ^{13}C-labeling patterns in shRNA control and AMPKα1/2 KD MDA-MB-231 cells or tumors. In summary, we obtained evidence from both MDA-MB-231 cultures and orthotopic tumors indicating that AMPK is a positive contributor to the following: (i) the Warburg effect; (ii) the nonoxidative PPC (Figs. 4 and 6). At the whole organism level, we also found AMPK-dependent effects of MDA-MB-231 tumor burden on glucose homeostasis in normal murine liver and pancreas (Fig. 7). As discussed below, these metabolic effects or mechanisms could in part explain how AMPK supports the development of orthotopic MDA-MB-231 tumors in nude mice.

In vitro metabolic profiling revealed that AMPK contributes significantly to core glucose metabolism in MDA-MB-231 cells (Fig. 4), but this contribution does not affect the proliferative or Warburg phenotype of these cells when cultured under nutrient-rich conditions (Figs. 2*B* and 5). Nevertheless, two important AMPK-dependent effects on glucose-derived carbon flow detected in cultures of MDA-MB-231 cells could provide a basis for understanding the contribution of AMPK to core glucose metabolism in MDA-MB-231 tumors (Fig. 6). First, the requirement for AMPK to sustain relatively high levels of extracellular lactate production (Fig. 4*C*), which is characteristic of the Warburg effect (1, 3), was retained in MDA-MB-231 (shRNA control) tumors (Fig. 6, *D* and *E*). Second, we obtained evidence that MDA-MB-231 tumors had a relatively greater preference for ribose synthesis through the nonoxidative compared with the oxidative PPC (Fig. 6*H*); this preference was also detected in MDA-MB-231 (shRNA control) cultures (Fig. 4*G*). These features of AMPK-dependent glucose metabolism in MDA-MB-231 cells, found both by *in vitro* and *in vivo* metabolic profiling, suggest that AMPK supports the development of MDA-MB-231 tumors in part by regulating glucose flux through aerobic glycolysis (producing lactate) and the PPC. At least for orthotopic MDA-MB-231 tumors, AMPK appears to contribute positively to the Warburg effect. In general, the role of AMPK in the Warburg effect in tumor cells is not clear; AMPK has been reported to be both a positive and negative regulator of this metabolic phenotype in various tumor cell types (31–33). Our findings suggest that direct or indirect targets of AMPK within the glycolytic pathway and the PPC determine its contribution to the Warburg effect and other phenotypes of tumor cell metabolism. In the glycolytic pathway, for example, AMPK has been reported to indirectly activate pyruvate dehydrogenase kinase leading to inhibition of pyruvate dehydrogenase (increasing lactate production) and to directly activate 6-phosphofructo-2-kinase leading to increased expression of the glycolytic activator fructose 2–6-bisphosphate (7, 33). The nonoxidative PPC, which produces pentose phosphates for nucleic acid synthesis, is primarily regulated by the thiamine diphosphate-dependent enzyme transketolase (TK) (34). It is possible that AMPK-dependent transketolase activity could underlie the effect of AMPKα1/2 KD on RNA-ribose synthesis in the nonoxidative PPC. The human genome contains one TK gene (*TKT*) and two TK-like genes (*TKTL1*, *TKTL2*); both TK and TK-like enzymes have been reported to support the development or maintenance of diverse human tumors (35–37).

In summary, *in vivo* metabolic profiling demonstrated that glucose metabolism in AMPKα1/2 KD compared with shRNA control MDA-MB-231 tumors resembled a non-Warburg phenotype, at least in terms of relatively diminished tissue lactate levels (Fig. 6, *D* and *E*). This conclusion suggests a plausible explanation for the relatively decreased growth of the AMPKα1/2 KD tumors found in this study (Figs. 2*A* and 6*B*), given that the Warburg effect is thought to support tumor development (1, 2). Thus, the "cryptic" AMPK-dependent effects on glycolysis and the PPC detected in conventional cultures of MDA-MB-231 cells may support the adaptation or survival of these cells in the metabolically stressed microenvironments of orthotopic tumors. However, establishing a causal relationship between such specific AMPK-dependent metabolic effects and the growth state of MDA-MB-231 tumors may not be straightforward. Metabolic profiling showed that MDA-MB-231 tumor burden in mice had substantial AMPK-dependent effects on glucose homeostasis in normal pancreas and liver (Fig. 7), indicating a systemic interaction between tumor and glucose-responsive normal tissues mediated in part by AMPK activity. Although this interaction might be attributed to the relatively high glucose demand of MDA-MB-231 tumors, as discussed under "Results," the level of ^{13}C-labeled plasma glucose was less in mice with AMPKα1/2 KD compared with

shRNA control tumors (Fig. 7*C*); there was higher circulating glucose in mice with wild-type tumors. Moreover, at the time of metabolic profiling, the AMPKα1/2 KD tumors had a mean volume only 25% smaller than that of the shRNA control tumors (Fig. 6*B*); this relatively small difference in mean tumor volume seems disproportionate to the relatively large differences in, for example, ribose synthesis shown in Fig. 7*A* for pancreas and liver in the same two groups of mice. Given the important role of AMPK in regulating whole-body energy metabolism by hormonal or endocrine signaling (6), it is plausible that AMPK activity in orthotopic MDA-MB-231 tumors could perturb glucose metabolism in sensitive normal tissues in a murine host through a circulating factor(s). This systems-level perspective implies that the metabolism of such MDA-MB-231 tumors could in turn be responsive to the state of whole-body energy homeostasis.

Progress in understanding the role of AMPK in human tumor biology will require expanded studies of AMPK biochemistry in diverse tumor cells and experimental tumor types. In this context, the discovery of specific small molecule AMPK inhibitors (currently available inhibitors are not highly specific for AMPK (38, 39)) could provide practical tool compounds in support of such studies.

REFERENCES

1. Vander Heiden, M. G., Cantley, L. C., and Thompson, C. B. (2009) Understanding the Warburg effect: the metabolic requirements of cell proliferation. *Science* **324,** 1029–1033
2. Schulze, A., and Harris, A. L. (2012) How cancer metabolism is tuned for proliferation and vulnerable to disruption. *Nature* **491,** 364–373
3. Metallo, C. M., and Vander Heiden, M. G. (2013) Understanding metabolic regulation and its influence on cell physiology. *Mol. Cell* **49,** 388–398
4. Hanahan, D., and Weinberg, R. A. (2011) Hallmarks of cancer: the next generation. *Cell* **144,** 646–674
5. Saggar, J. K., Yu, M., Tan, Q., and Tannock, I. F. (2013) The tumor microenvironment and strategies to improve drug distribution. *Front. Oncol.* **3,** 154
6. Hardie, D. G., Ross, F. A., and Hawley, S. A. (2012) AMPK: a nutrient and energy sensor that maintains energy homeostasis. *Nat. Rev. Mol. Cell Biol.* **13,** 251–262
7. Yuan, H. X., Xiong, Y., and Guan, K. L. (2013) Nutrient sensing, metabolism, and cell growth control. *Mol. Cell* **49,** 379–387
8. Laderoute, K. R., Amin, K., Calaoagan, J. M., Knapp, M., Le, T., Orduna, J., Foretz, M., and Viollet, B. (2006) 5′-AMP-activated protein kinase (AMPK) is induced by low oxygen and glucose deprivation conditions found in solid-tumor microenvironments. *Mol. Cell. Biol.* **26,** 5336–5347
9. Jang, T., Calaoagan, J. M., Kwon, E., Samuelsson, S., Recht, L., and Laderoute, K. R. (2011) 5′-AMP-activated protein kinase activity is elevated early during primary brain tumor development in the rat. *Int. J. Cancer* **128,** 2230–2239
10. Lehmann, B. D., Bauer, J. A., Chen, X., Sanders, M. E., Chakravarthy, A. B., Shyr, Y., and Pietenpol, J. A. (2011) Identification of human triple-negative breast cancer subtypes and preclinical models for selection of targeted therapies. *J. Clin. Invest.* **121,** 2750–2767
11. Physical Sciences-Oncology Centers Network, Agus, D. B., Alexander, J. F., Arap, W., Ashili, S., Aslan, J. E., Austin, R. H., Backman, V., Bethel, K. J., Bonneau, R., Chen, W. C., Chen-Tanyolac, C., Choi, N. C., Curley, S. A., Dallas, M., Damania, D., Davies, P. C., Decuzzi, P., Dickinson, L., Estevez-Salmeron, L., Estrella, V., Ferrari, M., Fischbach, C., Foo, J., Fraley, S. I., Frantz, C., Fuhrmann, A., Gascard, P., Gatenby, R. A., Geng, Y., Gerecht, S., Gillies, R. J., Godin, B., Grady, W. M., Greenfield, A., Hemphill, C., Hempstead, B. L., Hielscher, A., Hillis, W. D., Holland, E. C., Ibrahim-Hashim, A., Jacks, T., Johnson, R. H., Joo, A., Katz, J. E., Kelbauskas, L., Kesselman, C., King, M. R., Konstantopoulos, K., Kraning-Rush, C. M., Kuhn, P., Kung, K., Kwee, B., Lakins, J. N., Lambert, G., Liao, D., Licht, J. D., Liphardt, J. T., Liu, L., Lloyd, M. C., Lyubimova, A., Mallick, P., Marko, J., McCarty, O. J., Meldrum, D. R., Michor, F., Mumenthaler, S. M., Nandakumar, V., O'Halloran, T. V., Oh, S., Pasqualini, R., Paszek, M. J., Philips, K. G., Poultney, C. S., Rana, K., Reinhart-King, C. A., Ros, R., Semenza, G. L., Senechal, P., Shuler, M. L., Srinivasan, S., Staunton, J. R., Stypula, Y., Subramanian, H., Tlsty, T. D., Tormoen, G. W., Tseng, Y., van Oudenaarden, A., Verbridge, S. S., Wan, J. C., Weaver, V. M., Widom, J., Will, C., Wirtz, D., Wojtkowiak, J., and Wu, P. H. (2013) A physical sciences network characterization of non-tumorigenic and metastatic cells. *Sci. Rep.* **3,** 1449
12. Robey, I. F., Stephen, R. M., Brown, K. S., Baggett, B. K., Gatenby, R. A., and Gillies, R. J. (2008) Regulation of the Warburg effect in early passage breast cancer cells. *Neoplasia* **10,** 745–756
13. Jenkins, D. E., Hornig, Y. S., Oei, Y., Dusich, J., and Purchio, T. (2005) Bioluminescent human breast cancer cell lines that permit rapid and sensitive *in vivo* detection of mammary tumors and multiple metastases in immune deficient mice. *Breast Cancer Res.* **7,** R444–R454
14. Gucalp, A., and Traina, T. A. (2011) Triple-negative breast cancer: adjuvant therapeutic options. *Chemother. Res. Pract.* **2011,** 696208
15. Duellman, S. J., Calaoagan, J. M., Sato, B. G., Fine, R., Klebansky, B., Chao, W. R., Hobbs, P., Collins, N., Sambucetti, L., and Laderoute, K. R. (2010) A novel steroidal inhibitor of estrogen-related receptor α (ERRα). *Biochem. Pharmacol.* **80,** 819–826
16. Tomayko, M. M., and Reynolds, C. P. (1989) Determination of subcutaneous tumor size in athymic (nude) mice. *Cancer Chemother. Pharmacol.* **24,** 148–154
17. Stackpole, C. W. (1981) Distinct lung-colonizing and lung-metastasizing cell populations in B16 mouse melanoma. *Nature* **289,** 798–800
18. Lin, Z., Weinberg, J. M., Malhotra, R., Merritt, S. E., Holzman, L. B., and Brosius, F. C., 3rd. (2000) GLUT-1 reduces hypoxia-induced apoptosis and JNK pathway activation. *Am. J. Physiol. Endocrinol. Metab.* **278,** E958–E966
19. Laderoute, K. R., Calaoagan, J. M., Knapp, M., and Johnson, R. S. (2004) Glucose utilization is essential for hypoxia-inducible factor 1α-dependent phosphorylation of c-Jun. *Mol. Cell. Biol.* **24,** 4128–4137
20. Wise, D. R., DeBerardinis, R. J., Mancuso, A., Sayed, N., Zhang, X. Y., Pfeiffer, H. K., Nissim, I., Daikhin, E., Yudkoff, M., McMahon, S. B., and Thompson, C. B. (2008) Myc regulates a transcriptional program that stimulates mitochondrial glutaminolysis and leads to glutamine addiction. *Proc. Natl. Acad. Sci. U.S.A.* **105,** 18782–18787
21. Wu, M., Neilson, A., Swift, A. L., Moran, R., Tamagnine, J., Parslow, D., Armistead, S., Lemire, K., Orrell, J., Teich, J., Chomicz, S., and Ferrick, D. A. (2007) Multiparameter metabolic analysis reveals a close link between attenuated mitochondrial bioenergetic function and enhanced glycolysis dependency in human tumor cells. *Am. J. Physiol. Cell Physiol.* **292,** C125–C136
22. Cairns, R. A., Bennewith, K. L., Graves, E. E., Giaccia, A. J., Chang, D. T., and Denko, N. C. (2009) Pharmacologically increased tumor hypoxia can be measured by ^{18}F-fluoroazomycin arabinoside positron emission tomography and enhances tumor response to hypoxic cytotoxin PR-104. *Clin. Cancer Res.* **15,** 7170–7174
23. Boros, L. G., Cascante, M., and Lee, W. N. (2002) Metabolic profiling of cell growth and death in cancer: applications in drug discovery. *Drug Discov. Today* **7,** 364–372
24. Sonko, B. J., Schmitt, T. C., Guo, L., Shi, Q., Boros, L. G., Leakey, J. E., and Beger, R. D. (2011) Assessment of usnic acid toxicity in rat primary hepatocytes using ^{13}C isotopomer distribution analysis of lactate, glutamate and glucose. *Food Chem. Toxicol.* **49,** 2968–2974
25. Bhalla, K., Hwang, B. J., Dewi, R. E., Ou, L., Twaddel, W., Fang, H. B., Vafai, S. B., Vazquez, F., Puigserver, P., Boros, L., and Girnun, G. D. (2011) PGC1α promotes tumor growth by inducing gene expression programs supporting lipogenesis. *Cancer Res.* **71,** 6888–6898
26. Lee, W. N., Boros, L. G., Puigjaner, J., Bassilian, S., Lim, S., and Cascante, M. (1998) Mass isotopomer study of the nonoxidative pathways of the pentose cycle with [1,2-$^{13}C_2$]glucose. *Am. J. Physiol.* **274,** E843–E851
27. Boren, J., Cascante, M., Marin, S., Comín-Anduix, B., Centelles, J. J., Lim, S., Bassilian, S., Ahmed, S., Lee, W. N., and Boros, L. G. (2001) Gleevec

(STI571) influences metabolic enzyme activities and glucose carbon flow toward nucleic acid and fatty acid synthesis in myeloid tumor cells. *J. Biol. Chem.* **276,** 37747–37753
28. Hardie, D. G., and Pan, D. A. (2002) Regulation of fatty acid synthesis and oxidation by the AMP-activated protein kinase. *Biochem. Soc. Trans.* **30,** 1064–1070
29. Boros, L. G., Lerner, M. R., Morgan, D. L., Taylor, S. L., Smith, B. J., Postier, R. G., and Brackett, D. J. (2005) [1,2-$^{13}C_2$]Glucose profiles of the serum, liver, pancreas, and DMBA-induced pancreatic tumors of rats. *Pancreas* **31,** 337–343
30. Langlois, A. J., Holder, W. D., Jr., Iglehart, J. D., Nelson-Rees, W. A., Wells, S. A., Jr., and Bolognesi, D. P. (1979) Morphological and biochemical properties of a new human breast cancer cell line. *Cancer Res.* **39,** 2604–2613
31. Faubert, B., Boily, G., Izreig, S., Griss, T., Samborska, B., Dong, Z., Dupuy, F., Chambers, C., Fuerth, B. J., Viollet, B., Mamer, O. A., Avizonis, D., DeBerardinis, R. J., Siegel, P. M., and Jones, R. G. (2013) AMPK is a negative regulator of the Warburg effect and suppresses tumor growth *in vivo*. *Cell Metab.* **17,** 113–124
32. Liang, J., and Mills, G. B. (2013) AMPK: a contextual oncogene or tumor suppressor? *Cancer Res.* **73,** 2929–2935
33. Wu, C. A., Chao, Y., Shiah, S. G., and Lin, W. W. (2013) Nutrient deprivation induces the Warburg effect through ROS/AMPK-dependent activation of pyruvate dehydrogenase kinase. *Biochim. Biophys. Acta* **1833,** 1147–1156
34. Zhao, J., and Zhong, C. J. (2009) A review on research progress of transketolase. *Neurosci. Bull.* **25,** 94–99
35. Boros, L. G., Puigjaner, J., Cascante, M., Lee, W. N., Brandes, J. L., Bassilian, S., Yusuf, F. I., Williams, R. D., Muscarella, P., Melvin, W. S., and Schirmer, W. J. (1997) Oxythiamine and dehydroepiandrosterone inhibit the nonoxidative synthesis of ribose and tumor cell proliferation. *Cancer Res.* **57,** 4242–4248
36. Liu, H., Huang, D., McArthur, D. L., Boros, L. G., Nissen, N., and Heaney, A. P. (2010) Fructose induces transketolase flux to promote pancreatic cancer growth. *Cancer Res.* **70,** 6368–6376
37. Sun, W., Liu, Y., Glazer, C. A., Shao, C., Bhan, S., Demokan, S., Zhao, M., Rudek, M. A., Ha, P. K., and Califano, J. A. (2010) TKTL1 is activated by promoter hypomethylation and contributes to head and neck squamous cell carcinoma carcinogenesis through increased aerobic glycolysis and HIF1α stabilization. *Clin. Cancer Res.* **16,** 857–866
38. Bain, J., Plater, L., Elliott, M., Shpiro, N., Hastie, C. J., McLauchlan, H., Klevernic, I., Arthur, J. S., Alessi, D. R., and Cohen, P. (2007) The selectivity of protein kinase inhibitors: a further update. *Biochem. J.* **408,** 297–315
39. Viollet, B., Horman, S., Leclerc, J., Lantier, L., Foretz, M., Billaud, M., Giri, S., and Andreelli, F. (2010) AMPK inhibition in health and disease. *Crit. Rev. Biochem. Mol. Biol.* **45,** 276–295